Cryo-fracture TEM: direct imaging of viscous samples†

Alfredo González-Pérez* and Ulf Olsson

Received 22nd February 2008, Accepted 16th April 2008
First published as an Advance Article on the web 9th June 2008
DOI: 10.1039/b803115k

In the present work we show the capabilities of the new protocol called cryo-fracture TEM recently developed in our laboratory. The systems selected to test the protocol were $C_{12}E_8$–water and P84–water, and the phases imaged were lamellar (L_α), hexagonal (H_1) and cubic (I_1). This protocol is a natural extension of the capabilities of conventional cryo-TEM, which enables direct imaging of viscous samples.

Introduction

The use of electron microscopy (EM) techniques has become a conventional tool in order to elucidate self-assembled structures in soft matter. The characterization of the microstructure of those systems by EM techniques is a complement to scattering methods and can give additional valuable information not accessible by other methods. Currently, we can find two well-established EM techniques that can be used to image soft matter systems. Freeze-fracture electron microscopy (FFEM)[1–3] and cryogenic transmission electron microscopy (cryo-TEM).[4,5] In the first case, a liquid specimen is rapidly frozen and fractured to create a metal replica that can be imaged by EM. In the second, direct imaging of a vitrified sample is done. Both methods have advantages and disadvantages. The first one is especially useful in the case of highly viscous samples. However, in the case of more fluid samples the most recurrent is the cryo-TEM, that is the case for micelles, vesicles, tubules or any other structure stable in fluid solvents. The advantage of this protocol is that no replica of a frozen sample is needed (sometimes difficult to avoid artifacts) and hence the system can be imaged directly. The weak points are the extreme sensitivity of the sample to beam damage, which requires the use of a low-dose mode giving lower image resolution.

Different modifications of the cryoTEM protocol have been developed in order to expand their capability to more external conditions in which the protocol is not appropriate or essentially very weak. In some situations, the structure that should be imaged has a low contrast with respect to the bulk. This problem was partially solved by increasing the contrast on the sample by adding ammonium molybdate as a staining dye in a concentration on the order of *ca.* 16% (higher than the conventional negative-staining protocol that uses a concentration of *ca.* 2%). The protocol was called cryo-negative staining (cryo-NS) and is a simple and highly reproducible method that combines the conventional negative-staining (NS) protocol with cryo-TEM.[6,7] The disadvantage of this method is that in some cases the self-assembled structure is altered by the staining compound. More recently, a hybrid of both FFEM and cryo-TEM methods, called freeze-fracture direct imaging (FFDI),[8] has been developed and used successfully to image different systems. This protocol requires additional equipment. More information can be found in reports by Belkoura *et al.* and Agarwal *et al.*[8,9] There is a growing interest in imaging liquid crystals, not only because of their fundamental understanding, but also because of many industrial applications involving liquid-crystalline systems.[10] Danino *et al.* used conventional cryo-TEM experiments with a modification to perform the viscous phase on the grid to make the first direct images of hexagonal and cubic phases.[11] The protocol called "on-the-grid processing" was first proposed by Talmon *et al.* in 1996.[12] This method take the advantage of the know concentration gradient that exist in the thin layer sample going from the center to the wall of the holes in the grid. Obviously, this method is applicable only to low melting point systems.

Here we investigate an alternative method based on conventional cryo-TEM experiments that allows direct imaging of viscous systems.[13] The technique is called cryo-fracture transmission electron microscopy (cryo-fracture TEM). A thick film of the viscous sample is formed on the carbon grid. After vitrification, the carbon grid is punched with a needle to create perforations. The sample can be imaged by looking at the edges using an EM. This simple protocol was reported in a preliminary study that successfully used this to image a lamellar phase and a mesh phase characterized by the presence of bilayer perforations on the bilayers.[13] The cryo-fracture TEM protocol is expected to be a natural extension to the capabilities of conventional cryo-TEM that does not need additional equipment. The first detailed description of the protocol can be found in ref. 13.

In order to explore other viscous phases and demonstrate that cryo-fracture TEM is a powerful protocol in order to image viscous systems we have tested this protocol in two well-known binary non-ionic–water systems. The octaethylene oxide dodecylether ($C_{12}E_8$)–water system and the pluronic block copolymer P84–water system. The systems chosen present different viscous liquid-crystalline phases as a function of concentration close to room temperature. We can easily obtain Lamellar, cubic and hexagonal phases. The same phases in the $C_{12}E_8$ system have been studied earlier by Danino *et al.*[11] using cryo-TEM and the on-the-grid protocols.

Physical Chemistry 1, Center for Chemistry and Chemical Engineering, Lund University, P. O. Box 124, Lund, SE-22100, Sweden. E-mail: alfredo.gonzalez_perez@fkem1.lu.se; Fax: +46 46222 4413; Tel: +46 46222 8148

† A G.P wishes to dedicate this paper in memory of Prof. Jan Czapkiewicz from the Jagiellonian University, Kraków, Poland, a mentor and friend that recently passed away. "He strongly influenced my carrier, keeping alive my deep devotion for science."

Results and discussion

The phase behavior of polyoxyethylene surfactants in water is well known.[14] These systems are used in many applications as emulsifying agents and detergents, and are used as model systems to study different aspects of self-assembly structures. The rich morphologies we can obtain, based on such systems, include spherical micelles, thread-like micelles, lamellar, hexagonal, cubic and sponge phases. Additionally, they display the so-called intermediate structures, which is a challenge in understanding transitions between thermodynamically stable phases.[15,16]

In order to test the present protocol the non-ionic ($C_{12}E_8$)–water system was chosen. The phase diagram of the present system was reported in 1983 by Mitchell *et al.*[14] and later improved by others.[17–19] The phase diagram, redrawn from ref. 18, is shown in Fig. 1.

The phase diagram contains four different liquid-crystalline phases, found in the temperature range 15–20 °C. We prepared three concentrations forming lamellar (L_α), hexagonal (H_1) and a micellar cubic phase (I_1). The samples were left for several months before being imaged at the appropriate temperature to ensure the reorganization of the phases. We will present the results going from the highest to the lowest surfactant concentration following the series lamellar, hexagonal and cubic phases.

Lamellar phase

Following the phase diagram shown in Fig. 1, a lamellar phase was prepared. Imaging of lamellar phases often show some layers only when the orientation cuts perpendicularly to the stacked arrangement. In the present case, the $C_{12}E_8$ at 82 wt% and 20 °C was prepared. The results are shown in Fig. 2.

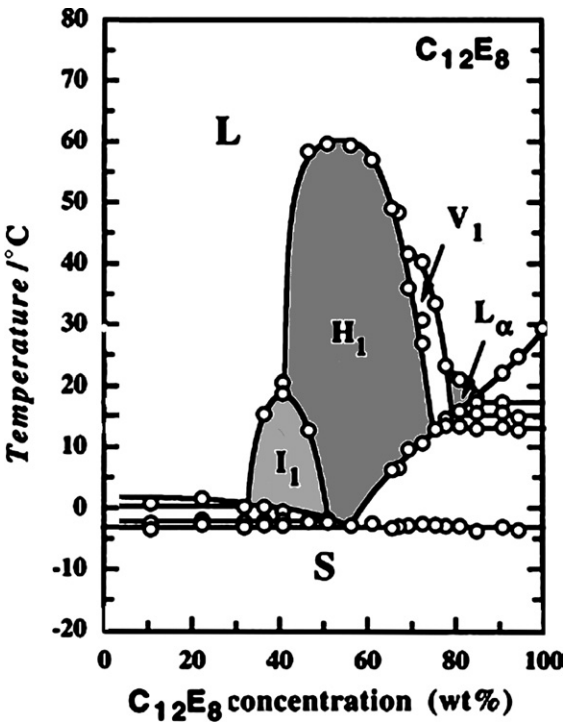

Fig. 1 Phase diagram for aqueous solutions of $C_{12}E_8$. Micellar region (L), micellar cubic phase (I_1), hexagonal phase (H_1), bicontinuous cubic phase (V_1), lamellar (L_α) and the solid phase (S) (redrawn from ref. 18).

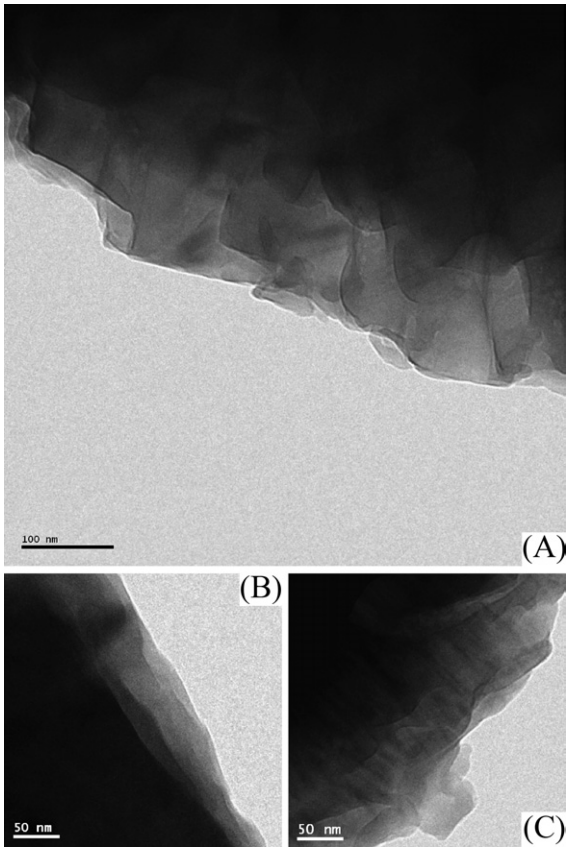

Fig. 2 A 82 %wt sample of $C_{12}E_8$ in water was prepared at 20 °C, resulting in a lamellar phase (L_α). Images performed by cryo-fracture TEM are shown in (A) (B) and (C) display the lamellar phase with some layers.

The stack of essentially flat extended bilayers, characteristic of the lamellar phase is easily seen. The images A, B and C (Fig. 2) were obtained at different fractures. Similar images were obtained earlier for the $C_{10}E_3$–water system.[12] Probably due to blotting, the lamellar phase is preferentially oriented with the bilayers parallel to the sample interface on the grid.[12]

Hexagonal phase

The hexagonal phase has a 2D hexagonal arrangement of long rod micelles. In order to perform the experiment we prepared a 52 wt% sample of $C_{12}E_8$ in water and it was left to equilibrate at 20 °C. The result for the hexagonal phase is shown in Fig. 3.

In Fig. 3, (A), (B) and (C) show the rod organization of the hexagonal phase. There is another orientation when the hexagonal phase is perpendicular to the orientation shown in the picture. This hexagonal arrangement is difficult to obtain because there is a preferential orientation of the rod on the grid. We chose a different region to perform the Fast Fourier transform (FFT) and an example is shown in Fig. 3(d). Masking the background we can perform the inverse of the FFT (IFFT) resulting in a cleaner image (see insert (e)) of the rod arrangement. From the FFT we obtain the characteristic distance of *ca.*

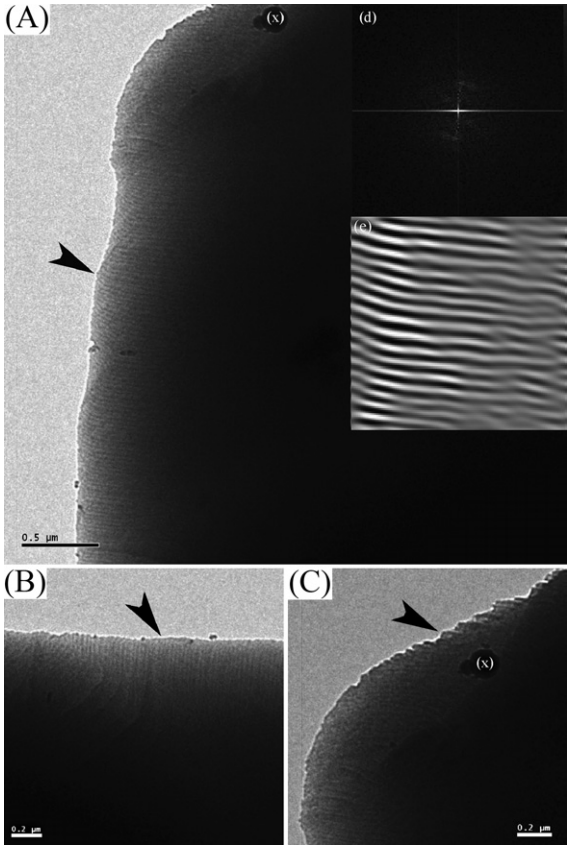

Fig. 3 Hexagonal phase (H_1) prepared form $C_{12}E_8$ at 52 %wt at 20 °C is shown. (A) shows a wide region with the hexagonal phase, and (B) and (C) show additional regions. The inserts (d) and (e) show, respectively, the FFT obtained from the region marked by the black arrow (A) and the resulting IFFT reconstruction after masking background. The (x) symbols show a form of crystalline ice on the top of the sample.

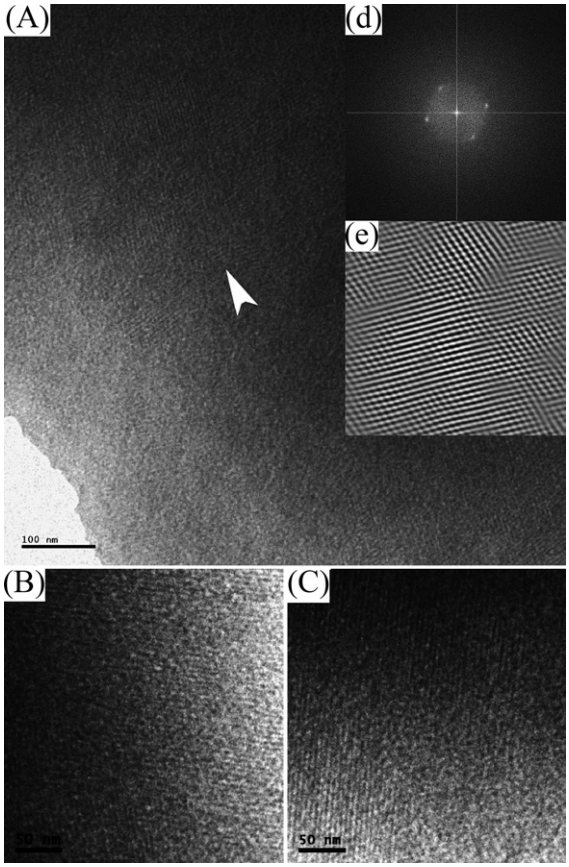

Fig. 4 Cubic phase (I_1), prepared with $C_{12}E_8$ at 40 wt% at 15 °C. (A) shows a wide area, and (B) and (C) show this in further detail. (B) and (C) represent the character. The inserts (d) and (e) show the FFT (from the region marked with the white arrow in (A)) and the reconstruction after masking the spots and doing IFFT, respectively.

0.5 nm. Carvell *et al.*[20] obtained a value of 0.6 nm for $C_{12}E_8$ at 52 %wt in water at 25 °C

Micellar cubic phase

The micellar cubic phase, which is of space group *Pm*3*n*, has a unit cell consisting of 8 closely packed slightly elongated micelles. A difficulty for the imaging of cubic phases is due to the small size of the micelles and also because the packed arrangement can be disturbed by blotting. In our case, a solution $C_{12}E_8$ at 40 wt% in water was prepared and left to equilibrate at 15 °C. The results for this cubic phase are shown in Fig. 4.

Fig. 4(A) shows a wide region with the cubic arrangement, and the insert on the right top corner shows the FFT (d) and the result of masking the noise and performing the IFFT (e). The results show the characteristic cubic arrangement. (B) and (C) shows more detailed images of such cubic arrangement in other fractured regions. The characteristic length scale in this structure is estimated to 1.5 nm from the FFT.

Pluronic block copolymer P84

The room temperature phase diagram of P84 in water have been reported by Alexandridis *et al.*[21] This block copolymer forms different liquid-crystalline phases and has a high melting point at high temperature. We prepared a concentration of 48 wt% P84 in water and left to equilibrate at 25 °C. At this concentration and temperature the system forms a hexagonal phase. This hexagonal phase is highly viscous and hence difficult to image by conventional cryo-TEM, and because of the high melting point it is not suitable for the on-the-grid crystallization method. In Fig. 5 we show the results obtained for this sample when prepared at 20 °C.

The repeat distance in the fracture is approximately 10 nm, in good agreement with ref. 21. Additionally, in the insert shown in (A) resulting from masking the noise and performing the IFFT we can observe dislocations on the arrangement indicated by a white arrow. This protocol can be used in combination with SAXS or SANS experiments in order to estimate the characteristic parameter of different liquid crystals giving a direct image of the arrangement.

Conclusions

Cryo-fracture TEM is a suitable protocol to image viscous systems. By exploring the present surfactant system, lamellar, hexagonal and cubic liquid-crystalline phases have been imaged with outstanding accuracy. The samples can be observed directly without the need for a replica (FFEM) or the on-the-grid

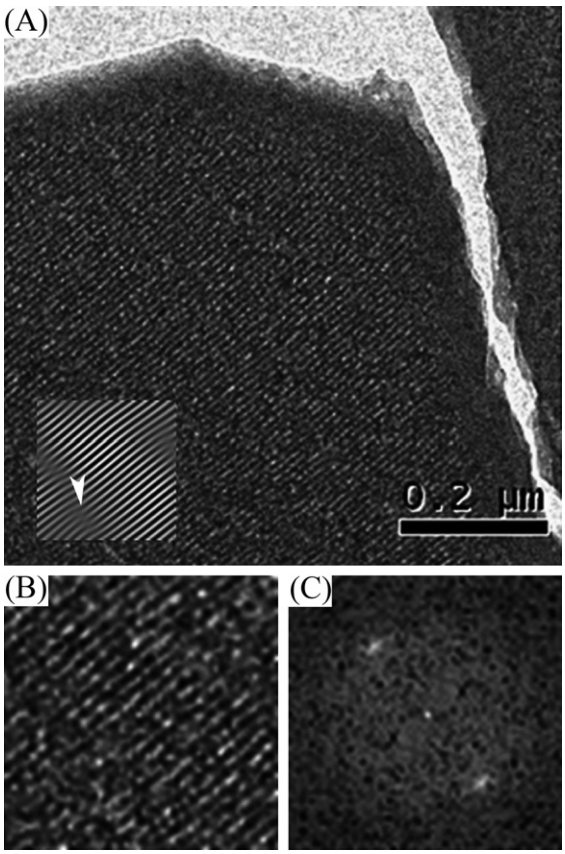

Fig. 5 Hexagonal phase (H_1), prepared with P84 at 48 wt% at 25 °C. (A) shows a wide area close to the fracture displaying the H1 phase. (B) shows the section used to perform the FFT shown in (C). The insert on (A) represents the reconstruction after masking the spots on (C) and performing IFFT.

protocol extension of conventional cryo-TEM protocol. No special equipment or complicated protocols are needed and the possibility to perform many perforations in a single carbon grid increases the chances of obtaining suitable thin areas. This protocol is a complementary method that extends the capabilities of the conventional cryo-TEM protocol allowing direct imaging of viscous systems.

Experimental

Materials

The surfactant octaethylene glycol mono-*n*-dodecyl ether ($C_{12}E_8$), with a purity of >98%, was purchased from Nikkol Chemicals Co. Ltd, Tokyo, and used as received. Pluronic P84 (EO_{19}–PO_{43}–EO_{19}) with molecular weight of 4200 g mol^{-1}, provided by BASF, was used without further purification. The $C_{12}E_8$ samples were prepared by gently mixing the appropriate amount of the surfactant (52, 40 and 81.5 wt%) and Millipore filtered water and then being left to equilibrate for several weeks. Each sample corresponds to a different phase: cubic (I_1), hexagonal (H_1) and lamellar (L_α).[18] In the case of P84, a concentration of 48 wt% was prepared in Millipore filtered water and left to equilibrate for several weeks to form a hexagonal phase (H_1).[22] The temperature was set using a thermostatic bath at 20 °C for H_1 and I_1 and at 15 C for the L_α according to the phase diagram shown in Fig. 1. The sample with P84 was kept at 25 °C. The samples were stored in a thermostatic bath at a given temperature until the moment they were transferred to the carbon grid. The samples were left to equilibrate for several weeks before any cryo-TEM experiments were done. Sample preparation and imaging were performed several times in order to check the reproducibility of the method.

Specimen preparation and fracturing

A preliminary study was previously published.[12] The specimens were prepared following a standard preparation procedure using a controlled environment vitrification system (CEVS)[23,24] thermostatted to the appropriate temperature. When samples are highly viscous, a critical step in the temperature control is the transfer of the sample from the water bath to the CEVS with a pipette. For a 15 °C sample, this step was done using a pre-cooled pipette. A small drop of the viscous sample was placed on the TEM grid covered with a lacy carbon film. The drop was then gently blotted to remove the excess sample and create as thin a layer of the sample as possible. The sample was kept on the CEVS for 10s to allow relaxation (reorganization of the structure). The grid containing the sample was plunged into liquid ethane (freezing point −180 °C) and then stored in liquid nitrogen (−196 °C).

Sample transfer is also a critical step in a similar way to conventional cryo-TEM experiments. Drying of the wet sample and heating of the vitrified sample were prevented by keeping the sample below −180 °C during each step and continuously, as in the conventional cryo-TEM protocol for specimen preparation. The vitrified sample was transferred to a liquid-nitrogen-cooled TEM cryo-holder (Oxford Instruments CT-3500) using a cryo-transfer station designed for minimal air exposure and heat loss. The set-up was a Philips CM120 BioTWIN BioCryo electron microscope operated at 120 kV. Images were recorded with a GIF 100 (Gatan Imaging Filter), using a CCD camera (MSC 791) in low-dose mode, giving a low electron-beam intensity of *ca.* 10 e^- per $Å^2$.[25] Imaging can be problematic if the carbon layer is also fractured because the support of the sample is then lost. The fractures can be created either by immediately plunging or before transfer into the microscope on the cryo-transfer station. Better fractures were obtained by making the fracturing the last step in the cryo-transfer station.

Artifacts and film thickness

Following the reported protocol, we should ensure that the film formed on the top of the carbon grid is thin enough to avoid melting. A suitable fracture should present a gradient in thickness enough to allow the beam to pass through. Fractures resulting in a sharp cut will not be appropriate to be imaged as they do not contain thin edges. Additionally, the melting of the sample inside the microscope can be observed in thick films that can not be observed in high magnification. In some cases by reducing the exposure time an appropriate image can be made even in thicker films. In Fig. 6 we show examples of different critical situations and some artifacts resulting mainly from a

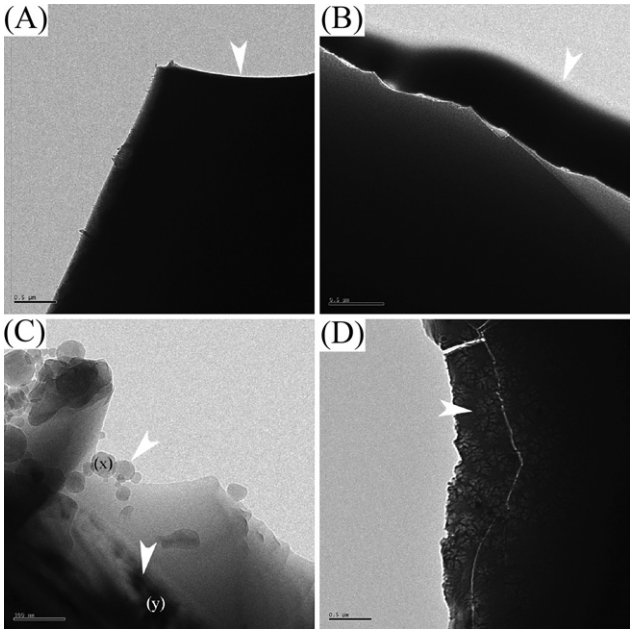

Fig. 6 (A) An example of a thick layer with a sharp break. In (B) we show melting of a layer that is too thick. We show frost (x) and crystalline ice (y) in (C). Sunflowers resulting from an inappropriate vitrification are shown in (D).

non-appropriate vitrification. We expect this to help in future developments.

Fig. 6(A) and 6(B) show non-appropriate sharp fracture and the melting resulting from the beam exposure in a thick film. Both cases are required to be avoided using this protocol. Even if the precise control of the sample thickness and the suitability of the fracture is difficult to obtain, a large number of fractures that can be created on the same carbon grid substantially increase the chances of having some suitable fractures. In (C) and (d) we show artifacts resulting in different ice forms. In (C) we show frost (x) and crystalline ice (y) present on the sample. As in conventional cryo-TEM experiments it is desirable to avoid such situation that can. In Fig. 6(D) we show the classical "sunflowers" resulting form a non-appropriate vitrification. This artifact is also known to form conventional cryo-TEM experiments.[5]

Acknowledgements

The authors are grateful to Gunnel Karlsson for helpful discussions and for skillful cryo-TEM imaging experiments. U.O thanks the Swedish Research Council (VR) for financial support.

References

1 T. Gulik-Krzywicki, *Curr. Opin. Colloid Interface Sci.*, 1997, **2**, 137–144.
2 H. W. Meyer and W. Richter, *Micron*, 2001, **32**, 615–644.
3 O. Mondain-Monval, *Curr. Opin. Colloid Interface Sci.*, 2005, **10**, 250–255.
4 M. Almgren, K. Edwards and G. Karlsson, *Colloids Surf., A*, 2000, **174**, 3–21.
5 H. Cui, T. K. Hodgdon, E. W. Kaler, L. Abezgauz, D. Danino, M. Lubovsky, Y. Talmon and D. J. Pochan, *Soft Matter*, 2007, **3**, 945–955.
6 M. Adrian, J. Dubochet, S. D. Fuller and J. R. Harris, *Micron*, 1998, **29**, 145–160.
7 C. El-Bez, M. Adrian, J. Dubochet and T. L. Cover, *J. Struct. Biol.*, 2005, **151**, 215–228.
8 L. Belkoura, C. Stubenrauch and R. Strey, *Langmuir*, 2004, **20**, 4391–4399.
9 V. Agarwal, M. Singh, G. McPherson, V. John and A. Bose, *Langmuir*, 2004, **20**, 11–15.
10 M. Malmsten, *Soft Matter*, 2006, **2**, 760–769.
11 D. Danino, Y. Talmon and R. Zana, *J. Colloid Interface Sci.*, 1997, **186**, 170–179.
12 Y. Talmon, *Ber. Bunsen-Ges. Phys. Chem.*, 1996, **100**, 364–372.
13 S. Bulut, A. Gonzalez-Perez and U. Olsson, *Langmuir*, 2008, **24**, 22–25.
14 D. J. Mitchell, G. J. T. Tiddy, L. Waring, T. Bostock and M. P. McDonald, *J. Chem. Soc., Faraday Trans. 1*, 1983, **79**, 975–1000.
15 S. Puntambekar, M. C. Holmes and M. S. Leaver, *Liq. Cryst.*, 2000, **27**, 743–747.
16 M. C. Holmes, *Curr. Opin. Colloid Interface Sci.*, 1998, **3**, 485–492.
17 M. Jonstromer, B. Jonsson and B. Lindman, *J. Phys. Chem. B*, 1991, **95**, 3293–3300.
18 L. Q. Zheng, M. Suzuki, T. Inoue and B. Lindman, *Langmuir*, 2002, **18**, 9204–9210.
19 L. Q. Zheng, M. Suzuki and T. Inoue, *Langmuir*, 2002, **18**, 1991–1998.
20 M. Carvell, D. G. Hall, I. G. Lyle and G. J. T. Tiddy, *Faraday Discuss. Chem. Soc.*, 1986, 223–237.
21 P. Alexandridis, U. Olsson and B. Lindman, *Langmuir*, 1998, **14**, 2627–2638.
22 B. Svensson, U. Olsson, P. Alexandridis and K. Mortensen, *Macromolecules*, 1999, **32**, 6725–6733.
23 J. R. Bellare, H. T. Davis, L. E. Scriven and Y. Talmon, *J. Electron Microsc. Tech.*, 1988, **10**, 87–111.
24 Y. Talmon, J. L. Burns, M. H. Chestnut and D. P. Siegel, *J. Electron Microsc. Tech.*, 1990, **14**, 6–12.
25 D. Danino, A. Bernheim-Groswasser and Y. Talmon, *Colloids Surf., A*, 2001, **183**, 113–122.